Nano Research

ISSN 1998-0124 CN 11-5974/O4
https://doi.org/10.1007/s12274-022-4797-1

Research Article

Direct growth of globally aligned graphene nanoribbons on reconstructed sapphire substrate using PECVD

Mingzhi Zou[1,§], Weiming Liu[1,§], Yue Yu[1], Shanshan Wang[2], Bo Xu[1], Liu Qian[1], Tianze Tong[1], and Jin Zhang[1] (✉)

[1] *College of Chemistry and Molecular Engineering, Beijing Science and Engineering Center for Nanocarbons, Beijing National Laboratory for Molecular Sciences, Peking University, Beijing 100871, China*
[2] *Science and Technology on Advanced Ceramic Fibers and Composites Laboratory, College of Aerospace Science and Engineering, National University of Defense Technology, Changsha 410000, China*
[§] *Mingzhi Zou and Weiming Liu contributed equally to this work.*

Received: 25 May 2022 / **Revised:** 28 June 2022 / **Accepted:** 20 July 2022

ABSTRACT

Graphene nanoribbons (GNRs) are regarded as an ideal candidate for beyond-silicon electronics. However, synthesis of aligned GNR arrays on insulating substrates with high efficiency is challenging. In this work, we develop a facile strategy, involving KOH pre-treatment and high-temperature annealing, to construct parallel steps on the two-fold symmetry a-plane sapphire substrate. Horizontal GNRs as narrow as 15.1 nm with global alignment across a region of 20 mm^2 are then grown on the step edge-enriched substrate through plasma enhanced chemical vapor deposition (PECVD) method. GNRs align well along the atomic steps on sapphire ([1$\bar{1}$00] direction) with their widths and densities swiftly adjustable by step morphology modification on substrate surface. A step-edge confined growth mechanism is proposed, attributing the constraint on the nanoribbon broadening to a relatively low growth temperature in PECVD, which restrains the activation energy to suppress GNRs across step edges on sapphire and prevents detrimental nanoribbon widening. The results provide a new perspective for scalable synthesizing well aligned nanoribbons of other two-dimensional materials.

KEYWORDS

graphene nanoribbon (GNR), global alignment, sapphire, insulating substrates, plasma enhanced chemical vapor deposition (PECVD)

1 Introduction

Graphene has numerous unique electronic [1], thermal [2], and optical properties [3], which attracts tremendous attentions in electronic applications. However, as a gapless material, although graphene has high carrier mobility, the low I_{ON}/I_{OFF} ratio limits its application in digital logic technology [4]. Fabricating graphene nanoribbon (GNR) through quantum confinement in one dimension is an effective approach to open the gap of graphene [5]. GNR is regard as one of the most ideal candidates to replace silicon for the next generation integrated circuits [6]. Due to the inverse relationship between width and bandgap of GNR [7], synthesizing narrower GNRs is the goal that scientists have been pursuing for decades. Meanwhile, scalable manufacturing GNR arrays with simpler and cheaper methods to realize large-scale applications is another significant target. At present, there are two main types of approaches to synthesize GNRs. One is the top-down synthetic strategy. GNRs are usually prepared by pattering graphene with lithographic techniques [8] or plasma etching treatments [9]. Unzipping carbon nanotubes to fabricated GNRs through plasma etching [10], chemical attack [11], high-pressure treatment [12], or metal nanoparticle catalyzed cutting [13] are also effective methods. However, GNRs manufactured by top-down strategies suffer from a high density of defects due to the harsh reaction conditions. The carbon atoms exposed during the treatment process can be oxidized easily, which usually results in unpredictable GNR edge structure and affects their conductive properties. Another class of approaches are bottom-up synthetic strategies. Specific small organic molecules with designed structure are evaporated onto clean noble metal surface and then converted into GNRs through dehalogenation and cyclodehydrogenation reaction with the catalysis of metal atoms under ultrahigh vacuum condition [14–16]. Although these methods can obtain GNRs with precise edge configuration and specific width, the expensive price of organic precursor and noble metal substrates restrict the large-scale synthesis of GNRs with these methods. Aside from these, the lengths of GNRs that fabricated by bottom-up synthetic strategies are always limited, which is difficult to meet the demands of electronic applications. Generally speaking, GNRs synthesized on metal film need to transfer onto insulating substrates to manufacture electronic devices. The transfer process usually introduces impurities and defects, and leads to the performance degradation of devices. Hence, developing methods for the batch production of GNRs directly on insulating substrates has great significance.

On top of these methods, there are some other growth strategies to synthesize GNRs. Liu et al. developed a template chemical vapor deposition (CVD) method, which utilized ZnS nanoribbons as templates to fabricate GNRs on them with CH_4

Address correspondence to jinzhang@pku.edu.cn

used as carbon source [17]. After the growth process, ZnS nanoribbons were etched by HCl solution to get suspended GNR membranes. Actually, using substrates with specific configuration (such as steps) as templates to grow GNRs is a common strategy. Michael et al. synthesized GNRs on Ge(001) surface with hill-and-valley structures [18]. The GNRs were grown on the terraces. Heer et al. manufactured nanometer-scale atomic steps on SiC crystal by fluorine-based reactive ion etching and induced the steps to relax to (1$\bar{1}$0n) facets by high-temperature annealing. GNRs were synthesized successfully on these steps with specific facets by heat treatment to 1,450 ℃ [19]. Zhang et al. also grew GNRs on hexagonal boron nitride substrates with atomic steps through plasma enhanced chemical vapor deposition (PECVD) method [20]. These approaches all clarify that using cramped substrates or fabricating confined step structures on substrates, and growing GNRs with substrate or step-edge confined growth strategies are effective. Nevertheless, these techniques either need complicated manufacturing and growth process or only achieve low production of GNRs. Scalable growth of globally aligned GNRs on insulated substrates with simple method and high efficiency is still a great challenge. According to the discussion above, designing a specific substrate with controlled crystallographic orientation parallel step structures to ensure the alignment of as-grown GNRs is probably an ingenious strategy to achieve scalable growth of globally aligned GNRs.

In this work, we developed a simple approach to reconstruct surface of sapphire with KOH pre-treatment and high-temperature annealing process, which can induce high-density parallel narrow atomic steps to form on the surface of sapphire. Next, high-density aligned cabined GNR arrays were grown on them with PECVD method. CH_4 was used as carbon source to take place of expensive organic molecules. The horizontal GNR arrays were grown on (11$\bar{2}$0) facets of sapphire and along the [1$\bar{1}$00] direction. The widths of GNRs are ranging from 15 to 60 nm approximately. With this approach, high-alignment cramped GNRs can be fabricated easily on insulating sapphire substrates and promote further applications of GNRs.

2 Results and discussion

The GNR arrays were grown with a radio frequency (RF, 13.56 MHz) PECVD system on a sapphire substrate at 850 ℃, as illustrated in Fig. 1(a). The plasma discharge source consisting of a copper coil wound around the outer wall of a 1-inch quartz tube was placed at the upstream of the furnace. The sapphire wafer was located at the high temperature zone that near the plasma discharge source. The plasma glow can reach the sapphire substrate when the plasma discharge source was turned on, as shown in Fig. S1 in the Electronic Supplementary Material (ESM). CH_4 was used as carbon source, and it can be decomposed effectively in plasma to provide enough high-activity carbon species for the growing process of GNRs. Before the process of growth, single-crystalline a-plane sapphire substrates were immersed into KOH solution to etch the surface and annealed at 1,100 ℃ subsequently to reconstruct their surface. Numerous aligned GNRs were grown on the newly formed parallel atomic steps of sapphire surface. Detailed growing procedures were described in Section 4. As a powerful approach to characterize structural and electronic properties of carbon materials, Raman spectroscopy was used to determine the composition of as-grown carbon materials. Figure 1(b) schemes the Raman spectra corresponding to bare sapphire and sapphire with the grown carbon materials, respectively. The carbon materials were grown when the PECVD system power was 20 W. Four Raman peaks were observed, including D peak at ~ 1,349 cm^{-1}, G peak at ~ 1,590 cm^{-1}, the D' peak at ~ 1,620 cm^{-1}, and the 2D peak at ~ 2,688 cm^{-1}. The result corresponds well with previous reports of GNR [10, 20, 21]. There is no radial breathing mode in the Raman spectrum of as-grown carbon materials on sapphire, which proves that no carbon nanotube exists. The scanning electron microscopy (SEM) image in Fig. 1(c) displays oriented, stripe-like carbon materials on reconstructed sapphire substrate. Combining the Raman spectra and SEM characterization results, we can get the conclusion that GNRs were synthesized successfully. It is worth noting that the power of the PECVD system has a major impact on the growth results by affecting the concentration of cracked carbon fragments. As the PECVD system power increases from 0

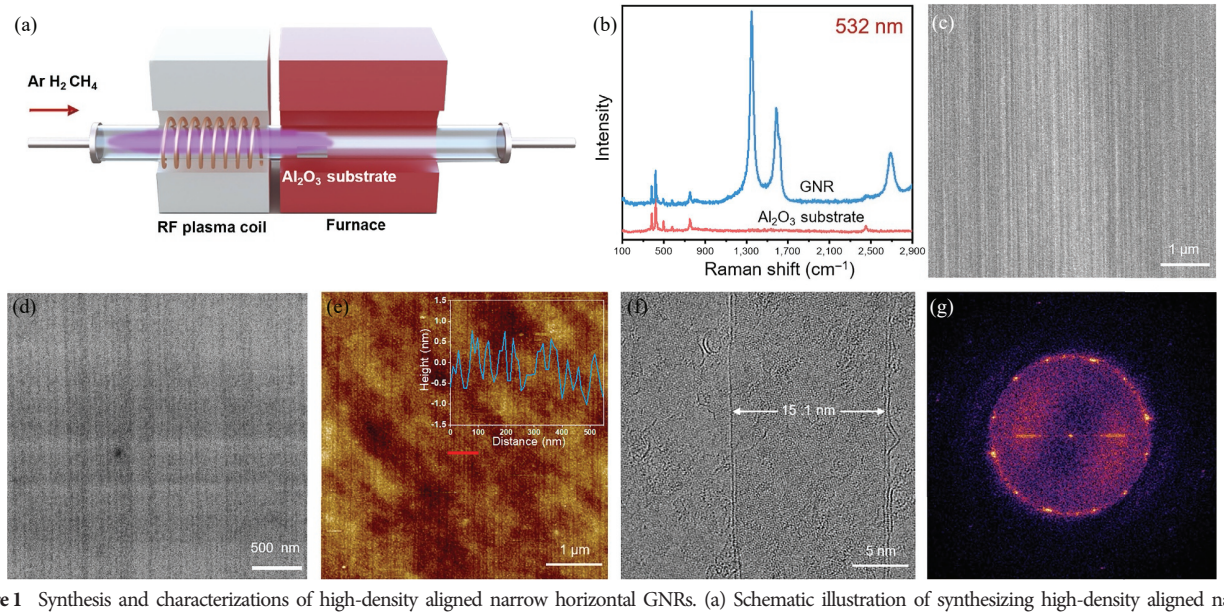

Figure 1 Synthesis and characterizations of high-density aligned narrow horizontal GNRs. (a) Schematic illustration of synthesizing high-density aligned narrow GNRs with PECVD on reconstructed sapphire substrate. (b) The Raman spectra of bare sapphire and GNR arrays grown on reconstructed sapphire substrate. (c) SEM image of high-density narrow GNR arrays grown on reconstructed sapphire substrate with parallel atomic step structures. (d) SEM image of high-density narrow GNR arrays which are transferred on plane SiO_2/Si substrate with the assistance of PMMA. (e) AFM image of high-density narrow GNR arrays which are transferred on plane SiO_2/Si substrate with the assistance of PMMA, inset is the height diagram of red line. (f) TEM image of GNR/graphene support membrane heterostructure on a holey SiN_x TEM grid. (g) FFT image of GNR in Fig. 1(f).

to 100 W, the carbon sources will be decomposed more thoroughly. Thus, an increased number of carbon fragments were collided, reacted, and deposited on the sapphire substrate, which induced different carbon materials to grow. As shown in Fig. S2(a) in the ESM, the sapphire substrates after growing process will be darker with the increasing of PECVD system power. When the PECVD system power is 0 W, there is nothing deposited on sapphire substrate because almost no carbon sources are cracked. The growth results on sapphire substrates change from carbon nanotubes at 10 W, to GNR arrays at 20 W, to amorphous carbon at 50 W, to vertical graphene at 100 W. Their SEM and corresponding Raman spectroscopy characterized results are illustrated in Figs. S2(b)–S2(f) in the ESM. Finally, we found that 20 W is a proper power for growing GNR arrays. Figures S3(a)–S3(c) in the ESM display SEM images of GNR arrays on reconstructed sapphire substrate with different magnifications. Figure S3(a) in the ESM exhibits that most of area on sapphire wafer (4 mm × 6 mm) is covered with GNR arrays (the white area is covered by GNR arrays), which verifies that this approach can achieve scalable growth of GNR arrays. To further characterize the width and density of horizontal GNR arrays and avoid the influence of atomic steps on sapphire surface on measuring results, the horizontal GNR arrays were transferred to plane SiO_2/Si substrate with the assistance of poly(methyl methacrylate) (PMMA). The SEM image of horizontal GNR arrays on SiO_2/Si substrate is shown in Fig. 1(d). And Fig. 1(e) shows the atomic force microscopy (AFM) image of horizontal GNR arrays on SiO_2/Si substrate. Apparent aligned array configuration is illustrated in Figs. 1(d) and 1(e) clearly, which proves that GNR arrays are synthesized successfully. The inset height diagram of Fig. 1(e) shows that the widths of GNRs are about 20–50 nm, and the density of GNR arrays is approximately 20 ribbons·μm^{-1}. The average length of GNRs is 2.5 ± 0.7 μm, as shown in Fig. S8(b) in the ESM. Transmission electron microscopy (TEM) was used to further characterize the width and crystal quality of GNR, as shown in Fig. 1(f). Due to the relatively confined and short size of GNRs, they cannot achieve self-support on normal holey silicon nitride (SiN_x) TEM grid. Thus, the GNRs need to be transferred on a holey SiN_x TEM grid with a support membrane to ensure GNRs can exist on the TEM grid. Previous work reported that single-layer graphene is an outstanding electronically transparent material which can serve as support membrane for TEM characterization [22]. Herein, the as-grown GNRs were transferred to a single-layer graphene with the assistance of PMMA. Then the GNR/graphene heterostructure was transferred to a holey SiN_x TEM grid for TEM characterization. It is clear that the width of GNR is 15.1 nm. Low magnification TEM image is shown in Fig. S3(d) in the ESM, which illustrates obvious strip configuration of GNR. The fast Fourier transform (FFT) image in Fig. 1(g) provides lattice information of as-grown GNR/graphene heterostructure in reciprocal space. There are several sets of reflexes in the image. To analyze the ascription of reflexes, we performed an in-depth analysis of GNR lattice structure, as shown in Fig. S4 in the ESM. Figure S4(a) in the ESM depicts FFT image of graphene support membrane area in Fig. 1(f) and Fig. S4(b) in the ESM shows the FFT image of GNR/graphene heterostructure area. There is only one set of reflexes in Fig. S4(a) in the ESM, which demonstrates that the single-layer graphene membrane is a single crystal. If we take Fig. S4(a) in the ESM as background and subtract signal of graphene support membrane in Fig. S4(b) in the ESM, the other reflexes belong to as-grown GNR. According to this information, we can infer that as-grown GNR is polycrystalline. The apparent equatorial line in reciprocal space and boundary structures in real space both verify the one-dimensional structure of GNR. The intensity distribution of other reflexes does not fit the Bessel function, which demonstrates that boundary structures are not carbon nanotube structures [23]. Although the reflexes in reciprocal space are brilliant, there is no apparent lattice structure in real space, which is due to residual impurities resulting from transfer process are hardly to eliminate and affect the contrast of image.

To verify high degree of alignment of horizontal GNR arrays, polarized Raman measurement was used to probe the global alignment of GNR arrays through rotating a $\lambda/2$ wave plate to change the polarization direction of incident light [24]. Figure 2(a) shows the fitted polarized Raman spectra of horizontal GNR arrays when the laser-Raman polarization rotates and at different angles (0°, 45°, and 90°) with the axial direction of GNRs. When the laser-Raman polarization is parallel to the GNR axial direction, we define this condition as zero degree. In that case, the Raman peaks of GNR reach maximum intensities. And when the laser-Raman polarization is perpendicular to the GNR axial direction (90°), the Raman peaks of GNR reach minimum intensities. Four Raman peaks are observed for GNR, including D peak at ~ 1,349 cm^{-1}, G peak at ~ 1,590 cm^{-1}, the D' peak at ~ 1,620 cm^{-1}, and the 2D peak at ~ 2,688 cm^{-1}. Other peaks on the Raman spectra belong to the sapphire substrate. The breathing modes of sp^2 rings result in appearing of D peak and they are usually related to the disorder of GNR, and D' peak corresponds to a double-resonance Raman mode related to disorder. The G peak can represent the graphitic degree of GNR, which is due to the E_{2g} photon at the Brillouin zone center. And 2D peak is due to an intervalley double-resonance Raman mode corresponding to the layer interaction [25]. It is plausible that the defects or adsorbates cause the high intensity of D peak (such as amorphous carbon formed by excessive carbon fragments collision in PECVD system). The high ratio between the intensity of D peak and G peak (I_D/I_G) may be due to the near armchair edge of GNRs [26, 27]. The four peaks all exhibit apparent polarization dependence, just as illustrated in Fig. 2(a). Figures 2(b)–2(d) and Fig. S5 in the ESM depict the Raman intensity plots of G peak, D peak, 2D peak, and D' peak in polar coordinates. These results show that the alignment of GNR arrays is excellent [21, 24]. Several different points were tested in different area on the reconstructed sapphire substrate where grew GNR arrays, and similar results were obtained and verified the global alignment of as-grown GNRs. It is worth noting that when the laser-Raman polarization is parallel to the [1$\bar{1}$00] direction (sapphire substrates in our experiment were cut along [1$\bar{1}$00] direction), the intensities of four peaks correspond to GNRs exhibit maximum value. This result indicates that the growth behavior of GNRs is closely related to crystallographic orientation of sapphire substrates. Thus, we performed exhaustive characterizations of reconstructed sapphire structure to explore the relationship between them.

The key point to grow GNR arrays is to choose a proper substrate. According to previous work of synthesizing GNR, we found that manufacturing nanofacets or step structures is an effective strategy [19]. Referring the experience of growing carbon nanotube arrays on sapphire substrate, which can align carbon nanotube with abundant atomic steps on it [28], we decided to choose a-plane sapphire as the substrate to grow horizontal GNR arrays. A-plane sapphire substrates in our experiments were purchased from Hefei Kejing Materials Technology Co., Ltd, China. Their surface roughness is usually less than 5 Å, and miscut angle is less than 0.5°. Figure 3(a) shows the AFM image of a-plane sapphire surface after cleaning, which is a continuous plane surface without apparent step structures. High-temperature annealing is a commonly used approach to relax lattice stress and induce the formation of low-energy facets. The a-planes of sapphire are (11$\bar{2}$0) facets, which have higher energy than (0001)

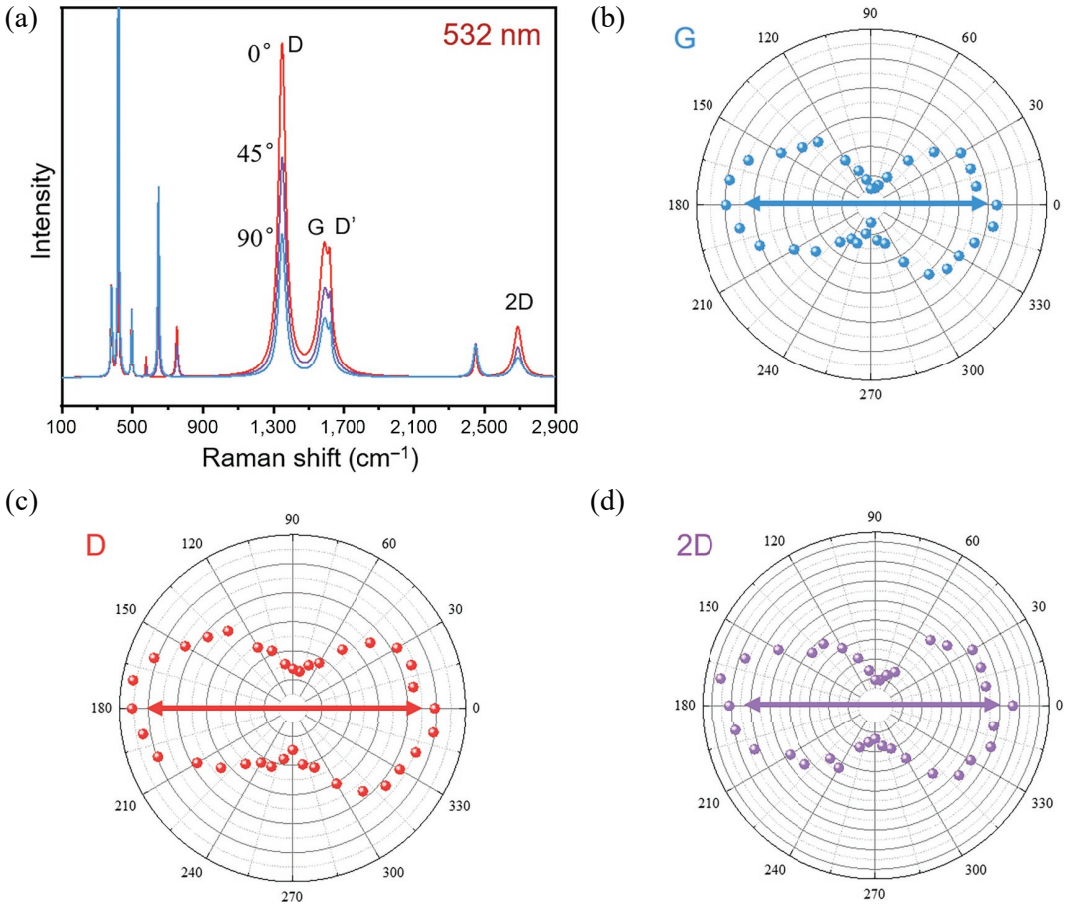

Figure 2 Polarized Raman spectra of global aligned horizontal GNR arrays on reconstructed sapphire substrate. (a) Polarized Raman spectra of global aligned GNR arrays on reconstructed sapphire substrate when the laser-Raman polarization was at different angles to the axial direction of GNRs. (b) Polar plot of the G peak intensities. (c) Polar plot of the D peak intensities. (d) Polar plot of the 2D peak intensities (the 0° in polar plots is the condition that laser-Raman polarization is parallel to [1$\bar{1}$00] direction of sapphire).

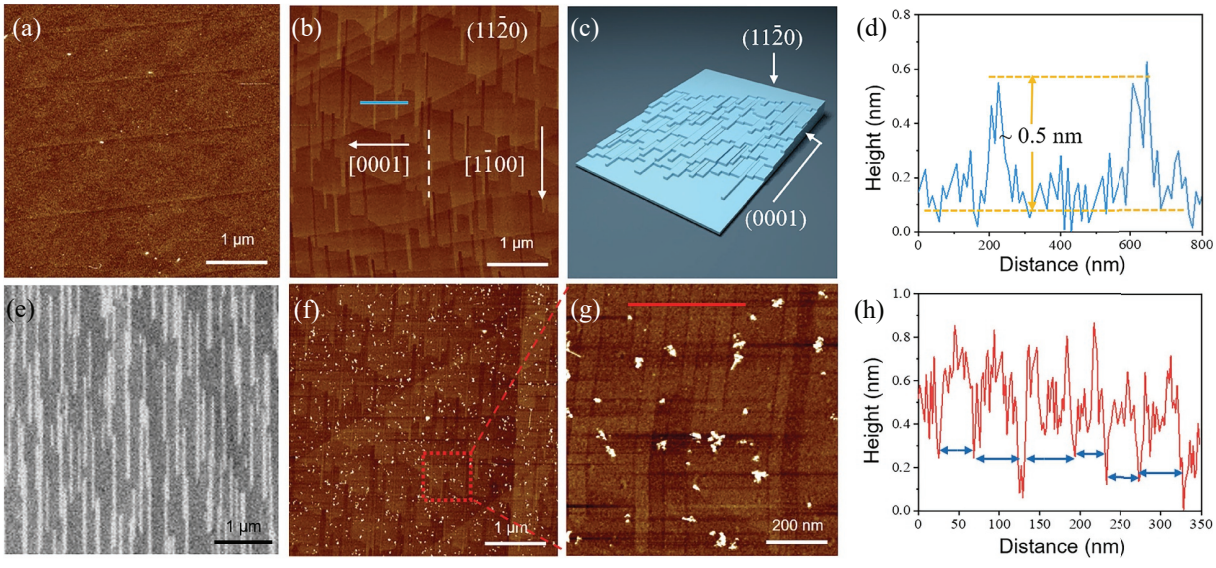

Figure 3 Reconstruction of sapphire substrate through high-temperature annealing process and characterizations of GNR arrays grown on reconstructed sapphire substrate. (a) AFM image of sapphire substrate after cleaning. (b) AFM image of sapphire substrate after a high-temperature annealing process. (c) 3D structure of reconstructed sapphire surface. (d) Height diagram of blue line in Fig. 3(b), which illustrates heights and widths of two typical atomic steps on reconstructed sapphire. (e) SEM image of horizontal GNR arrays grown on reconstructed sapphire substrate. (f) AFM image of reconstructed sapphire surface after the growth of horizontal GNR arrays. (g) Zoomed-in image of the red square box in Fig. 3(f). (h) Height diagram of red line in Fig. 3(g), which illustrates widths and heights of several horizontal GNRs.

facets (c-plane). (0001) facets are perpendicular to (11$\bar{2}$0) facets and parallel to [1$\bar{1}$00] direction. Via a 1,100 °C-annealing process, lots of new (0001) facets form along the [1$\bar{1}$00] direction and separate (11$\bar{2}$0) facet into parallel cramped long strips, as illustrated in Fig. 3(b), respectively [29, 30]. Figure 3(c) depicts the three-dimensional (3D) structure of reconstructed sapphire surface after high-temperature annealing. The strips in Fig. 3(b) actually are step configurations on substrate surface, whose top planes are (11$\bar{2}$0) facets, and the cross-section planes parallel to [1$\bar{1}$00] direction are (0001) facets. The formation of new (0001) facets is

the main reason that numerous atomic steps appear on the reconstructed sapphire surface, and these steps provide growth sites for GNRs. The height of every atomic step is approximately 0.5 nm, as schemed in Fig. 3(d), which depicts the height diagram of blue line in Fig. 3(b). The blue line spans two typical atomic steps. The widths of atomic steps on sapphire surface are not uniform, and the average width is 57.6 ± 21.7 nm, as show in Fig. S7(a) in the ESM. The Fig. 3(e) shows the typical SEM image of GNR arrays grown on reconstructed sapphire via high-temperature annealing. It is clear that there are many aligned white strips grown on the surface of substrate. Figure 3(f) illustrates AFM image of GNR arrays grown on reconstructed sapphire. Compared with Fig. 3(b), we can see that there are many cramped strips grown on the step structures. The edges of strips are more apparent than the step structures in Fig. 3(b), and they are GNRs. The nanoparticles deposited on sapphire surface are amorphous carbon formed by superfluous cracked carbon species in PECVD system. For convenience of observation, we selected an area where GNRs are apparent and dense to zoom-in. Figure 3(g) schemes the zoomed-in picture of red square box area in Fig. 3(f). Obviously, there are several parallel strips on the substrate surface. The average height of strips is 0.4 nm and average width is 50.7 nm, which proves that the GNRs are single layer [31], as shown in Fig. 3(h). To further verify that GNRs were synthesized successfully, the sample was transferred to plane SiO_2/Si substrate with the assistance of PMMA, as shown in Fig. S6 in the ESM. There are still white strips on the substrate, which proves the successful growth of GNRs. Careful examination shows that the widths of GNRs are similar to the widths of atomic steps on reconstructed sapphire. Most of GNRs are grown on the parallel atomic steps along the [1$\bar{1}$00] lattice direction of a-sapphire, so the growth direction of GNRs is [1$\bar{1}$00] lattice direction of a-sapphire, which results in the high degree of alignment of horizontal GNR arrays. Given that step edges usually have high surface energy and can absorb highly-active carbon fragments easily, parallel step structures of reconstructed sapphire could be the key point to achieve the growth of globally aligned horizontal GNRs that have close correlation with the step width.

To confirm our hypothesis and achieve the target of synthesizing narrower GNRs, we developed a KOH pre-preparation strategy to decrease the widths of atomic steps on reconstructed sapphire surface and increase the density of them. Before the high-temperature annealing process, a-plane sapphire substrates were immersed into KOH solution for 48 h. Figure 4(a) depicts the AFM image of a-plane sapphire surface after KOH treatment. KOH etches the sapphire surface and induces some short narrow strips to form. Because the rates of KOH etching are different for different facets on sapphire surface, some new facets exposed during the KOH etching process. Combined with the 3D structure in Fig. 3(c) to analyze, we can find that some (0001) facets are formed after KOH treatment, and provided initial seeds for anneal process. Higher density and narrower step configurations are formed after high-temperature annealing process, as illustrated in Fig. 4(b). The AFM image of new reconstructed sapphire shows that there are much more restricted atomic steps compared with sapphire without KOH pre-treatment in Fig. 3(b). Figure 4(c) shows high-density aligned horizontal GNRs grown on reconstructed sapphire substrate with KOH pre-treatment. Corresponding SEM and AFM characterizations are displayed in Figs. 1(c)–1(e). To investigate the relationship between as-grown GNRs and step structures, we counted the widths and numbers of them in unit area on reconstructed sapphire without or with KOH pre-treatment. The statistical data are shown in Fig. 4(d) and the detail data are illustrated in Fig. S7 in the ESM. The average width of steps and GNRs without KOH pre-treatment are 57.6 ± 21.7 and 54.2 ± 17.1 nm, respectively. The average width of steps and GNRs with KOH pre-treatment are 27.9 ± 10.3 and 24.5 ± 9.0 nm, respectively. According to the histogram in Fig. 4(d), we can find that widths and numbers of GNRs have positive correlation with atomic steps on the substrate surface. The GNR mean widths are similar to the mean widths of steps on reconstructed sapphire substrate. Through KOH etching process, the width of step structures on reconstructed substrate becomes more restricted, and the width of GNRs also becomes cramped, which is still comparable with atomic steps. The relationship between the density of GNRs and atomic steps on reconstructed sapphire substrates is similar without or with KOH pre-treatment. We also measured the mean length of GNRs grown on reconstructed sapphire without or with KOH pre-treatment. The detail statistical data are shown in Fig. S8 in the ESM, and the average lengths of GNRs grown on reconstructed sapphire without or with KOH pre-treatment are 1.6 ± 0.5 and 2.5 ± 0.7 μm, respectively. If we add a KOH pre-treatment process before high-temperature annealing, KOH will etch the sapphire

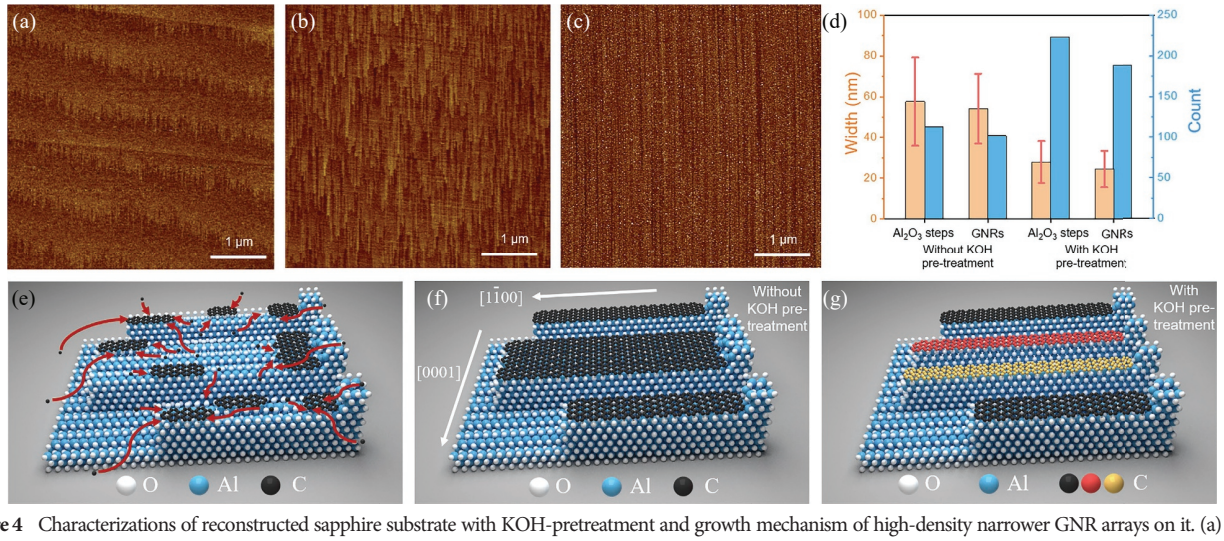

Figure 4 Characterizations of reconstructed sapphire substrate with KOH-pretreatment and growth mechanism of high-density narrower GNR arrays on it. (a) AFM image of sapphire substrate after KOH pre-treatment. (b) AFM image of sapphire substrate after KOH pre-treatment and high-temperature annealing. (c) AFM image of high-density narrower horizontal GNR arrays grown on new reconstructed sapphire substrate. (d) Statistical data of width and number of steps and GNRs in unit area on reconstructed sapphire substrate without or with KOH pre-treatment. (e) and (g) Growth mechanism of horizontal GNR arrays on high-density parallel step structures of reconstructed sapphire substrate without or with KOH pre-treatment. The KOH pre-treatment induces sapphire to form much more restricted step structures after high-temperature annealing process, which results in much more cramped GNR grown on reconstructed sapphire substrate.

surface which induces some short narrow steps to form during this pre-treatment process. So compared with step structures formed without KOH pre-treatment, the steps formed with KOH pre-treatment are longer. The lengths of atomic steps also affect the lengths of GNRs. Based on this result, we proposed a model to elucidate the step-edge confinement effect on the growth of GNRs. Figures 4(e)–4(g) clarify the growth mechanism of horizontal GNR arrays on reconstructed sapphire surface. Initially, the edges of atomic steps which have high surface energy catch the highly-active carbon species that are fully decomposed in PECVD system and form initial seeds of graphene. Then these seeds function as nucleus and adsorb decomposed carbon fragments for the growth of graphene, as illustrated in Fig. 4(e). Several graphene islands will merge and form large area graphene domains as the reaction time increased. Because of a relatively low growth temperature compared to those in normal CVD processes for graphene growth, when the graphene domains expand and their boundaries coincide with the boundary of the step edges, they do not have enough energy to grow across steps on reconstructed sapphire surface. The growth process of graphene domain along [0001] direction of sapphire stopped, but the growth along [$1\bar{1}00$] direction continued. Finally, horizontal GNRs with width similar to that of the surface steps were grown on reconstructed sapphire surface. Due to the randomness of nucleation at the edges of sapphire atomic steps, different domains usually have unidirectional alignment. So almost as-grown GNRs are polycrystalline, as TEM characterization demonstrated. If the step width on a-sapphire is not controlled, some relatively wide GNRs will grow on wide atomic steps of reconstructed sapphire substrates without KOH pre-treatment, as depicted in Fig. 4(f). If the sapphire substrate is etched by KOH before the high-temperature annealing process, some wide steps will be divided into several narrower steps by newly formed (0001) facets during the high-temperature annealing process. The widths of GNRs decrease according to the growth mechanism clarified above, as exhibited in Fig. 4(g). The red and yellow GNRs in Fig. 4(g) have more cabined width compared to original black GNR in Fig. 4(f). Meanwhile, the density of horizontal GNR arrays will be higher with the increase of atomic step density. This strategy to reconstruct sapphire surface and fabricate abundant step configurations is also likely to synthesize other two-dimensional material nanoribbons with global alignment.

3 Conclusion

In summary, we designed a simple KOH pre-treatment and high-temperature annealing strategy, manufactured surface reconstructed sapphire with high-density parallel narrow step configurations and achieved growth of high-density globally aligned horizontal GNR arrays on insulating sapphire substrates with PECVD. Polarized Raman characterization verifies the global alignment of as-grown GNRs on reconstructed sapphire. SEM and AFM characterizations demonstrate that the fabricated GNR arrays have high density. TEM characterization proves the cramped width of GNRs (15.1 nm). Through investigating the relationship between the step structures on sapphire and GNRs, a step-edge confined growth mechanism was proposed to clarify the growth process of aligned GNRs. This work not only demonstrates a cheap and efficient method to fabricate highly aligned horizontal GNR arrays on insulating substrates without expensive organic molecules and noble metal substrates, but also provides a new perspective for synthesizing two-dimensional material nanoribbons on substrates with step configurations through simple CVD method.

4 Methods

4.1 Preparation of reconstructed sapphire substrate (without KOH treatment)

In our experiments, we used a-plane sapphire substrates (single-side polished, surface roughness < 5 Å, miscut angle < 0.5°) purchased from Hefei Kejing Materials Technology Co., Ltd, China as substrates for growing GNR arrays. Before the growth process, the sapphire substrates must be ultrasonic cleaned with deionized water, followed by acetone, ethanol, and deionized water again for 15 min. Next, the cleaned sapphire substrates were sent into a muffle furnace and annealed at 1,100 °C in air for 8 h to reconstruct the surface and form parallel step structures.

4.2 Preparation of reconstructed sapphire substrate (with KOH treatment)

Typically, 33.66 g KOH was dissolved in 200 mL deionized water to get 3 M KOH aqueous solution. A-plane sapphire substrates were immersed in 3 M KOH solution for 48 h. Afterwards, the sapphire substates must be ultrasonic cleaned with deionized water twice to remove residuals left by the etchant, then followed by acetone, ethanol, and deionized water for 15 min. Next the cleaned sapphire substrates were sent into a muffle furnace and annealed at 1,100 °C in air for 8 h to reconstruct the surface and form narrower parallel step structures.

4.3 Synthesis of aligned horizontal GNR arrays on reconstructed sapphire substrates with PECVD method

The reconstructed sapphire substrate was located about 8 cm upstream of reactor furnace center, which is near the plasma discharge source. The furnace was heated to 850 °C with a heating rate of 20 °C·min^{-1}. 300 standard cubic centimeters per minute (sccm) argon and 300 sccm hydrogen were purged into the tube during the heat process. When heated to set temperature (850 °C), the tube was pumped to vacuum, and flow of 30 sccm argon, 15 sccm hydrogen, and 2 sccm methane was introduced for the growth of GNR arrays, subsequently. Next, the plasma discharge source (the power was set as 20 W) was turned on. When the plasma glow was stabilized, the 10 min-growth process was started. Finally, the plasma discharge source was turned off and stopped to purge methane into tube to end the growth process. The furnace was cooled to room temperature in an argon and hydrogen flow afterwards. All gas flows into the reactor were controlled with mass flow controllers (MFCs).

4.4 General characterizations

SEM images were obtained on a Hitachi S4800 SEM operated at 1.0 and 10 kV. Raman spectra of GNR arrays were collected by Jovin Yvon–Horiba LabRam systems with 532 nm excitation laser. AFM images were obtained using a Dimension Icon microscope (Bruker).

4.5 Polarized Raman characterizations

Polarized Raman spectra of GNR arrays were collected by JY Horiba HR800 Raman spectrometer with 532 nm excitation laser. Polarized light was produced by a linear polarizer and $\lambda/2$ wave plate for incidence. Rotated laser-Raman polarization from 0° to 360° was achieved by rotating $\lambda/2$ wave plate.

4.6 Transfer of GNR arrays onto SiO_2/Si (300 nm SiO_2) for SEM and AFM characterizations

A PMMA solution (950 K, 4 wt.%, from Allresist GmbH,

Germany) was spin coated onto the sapphire substrate with as-grown GNR arrays and then baked at 180 °C for 10 min until a thin film encapsulating the GNR arrays formed. The PMMA/GNRs film was exfoliated from the reconstructed sapphire surface by immersing in KOH aqueous solution (1 M, 70 °C) for 20 min. The PMMA/GNR film would be detached from the substrate as the sapphire was etched by KOH. The film was transferred and floated onto deionized water several times to remove residuals left by the etchant. Afterwards, the PMMA/GNRs film was attached to a SiO_2/Si substrate. The sample was then dried on the hotplate at 60 °C. Finally, the sample was immersed in acetone for 8 h to remove PMMA.

4.7 Transfer of GNR arrays onto SiN_x grid for TEM characterizations

The GNR/graphene heterostructure was constructed by wet transfer with the help of PMMA, in which a single layer graphene was used as an electronically transparent supporting membrane. Then, the constructed heterostructure could continue to be transferred to holey SiN_x TEM grid (from Norcada Inc., Canada) for TEM characterization. For polymer-supported transfer, the surface of CVD-grown GNR on the substrate (GNRs/Al_2O_3) was spin coated with the PMMA solution (950 K, 4 wt.%, from Allresist GmbH, Germany) and heated to dry on the hotplate at 180 °C for 10 min. The final thickness of the PMMA film was about 250 nm. Then, the sample was immersed in 1 M KOH aqueous solution to etch the sapphire substrate and the PMMA/GNR film would be detached from the substrate. Next, the detached PMMA/GNR film was transferred and floated onto deionized water several times to remove residuals left by the etchant. After cleaning, the copper foil on which a single layer graphene has been grown was used to scoop up the film from the water. The sample was then dried on the hotplate at 60 °C. Then the copper foil was etched away with 1 M $FeCl_3$ solution, and after a similar cleaning process using deionized water, the sample was scooped up by a holey SiN_x TEM grid. The sample was dried in air naturally, and then baked at 180 °C for 20 min. Finally, before TEM characterization, the sample was immersed in acetone for 8 h to remove PMMA.

TEM imaging was conducted on a Titan Cubed Themis G2 300 fitted with probe and image aberration correctors under an accelerating voltage of 300 kV. Images were recorded using a Gatan OneView CCD camera with 1 s acquisition time. The electron dose rate used for imaging was approximately 0.05 pA·nm^{-2}.

Acknowledgements

This work was financially supported by the Ministry of Science and Technology of China (Nos. 2016YFA0200100 and 2018YFA0703502), the National Natural Science Foundation of China (Nos. 52021006, 51720105003, 21790052, and 21974004), the Strategic Priority Research Program of Chinese Academy of Sciences (No. XDB36030100), and the Beijing National Laboratory for Molecular Sciences (No. BNLMS-CXTD-202001).

Electronic Supplementary Material: Supplementary material (photo of radio frequency PECVD system, SEM and Raman spectroscopy characterizations of different growth results when the PECVD system power is changed, SEM and TEM images of GNR at different magnifications, FFT image of different zones in Fig. 1(f), Polar plot of the D' mode intensity, SEM image of GNR arrays grown on reconstructed sapphire (without KOH pre-treatment) which is transferred on SiO_2/Si substrate, the detailed statistical data of steps and GNRs (widths and numbers) in 25 μm^2 on reconstructed sapphire without or with KOH pre-treatment, and the detailed statistical data of GNR lengths on reconstructed sapphire without or with KOH pre-treatment) is available in the online version of this article at https://doi.org/10.1007/s12274-022-4797-1.

References

[1] Zhang, Y. B.; Tan, Y. W.; Stormer, H. L.; Kim, P. Experimental observation of the quantum Hall effect and Berry's phase in graphene. *Nature* **2005**, *438*, 201–204.

[2] Chen, S. S.; Wu, Q. Z.; Mishra, C.; Kang, J.; Zhang, H. J.; Cho, K.; Cai, W. W.; Balandin, A. A.; Ruoff, R. S. Thermal conductivity of isotopically modified graphene. *Nat. Mater.* **2012**, *11*, 203–207.

[3] Liu, M.; Yin, X. B.; Ulin-Avila, E.; Geng, B. S.; Zentgraf, T.; Ju, L.; Wang, F.; Zhang, X. A graphene-based broadband optical modulator. *Nature* **2011**, *474*, 64–67.

[4] Schwierz, F. Graphene transistors. *Nat. Nanotechnol.* **2010**, *5*, 487–496.

[5] Yazyev, O. V. A guide to the design of electronic properties of graphene nanoribbons. *Acc. Chem. Res.* **2013**, *46*, 2319–2328.

[6] Liao, A. D.; Wu, J. Z.; Wang, X. R.; Tahy, K.; Jena, D.; Dai, H. J.; Pop, E. Thermally limited current carrying ability of graphene nanoribbons. *Phys. Rev. Lett.* **2011**, *106*, 256801.

[7] Wassmann, T.; Seitsonen, A. P.; Saitta, A. M.; Lazzeri, M.; Mauri, F. Structure, stability, edge states, and aromaticity of graphene ribbons. *Phys. Rev. Lett.* **2008**, *101*, 096402.

[8] Masubuchi, S.; Ono, M.; Yoshida, K.; Hirakawa, K.; Machida, T. Fabrication of graphene nanoribbon by local anodic oxidation lithography using atomic force microscope. *Appl. Phys. Lett.* **2009**, *94*, 082107.

[9] Liu, L.; Zhang, Y. L.; Wang, W. L.; Gu, C. Z.; Bai, X. D.; Wang, E. G. Nanosphere lithography for the fabrication of ultranarrow graphene nanoribbons and on-chip bandgap tuning of graphene. *Adv. Mater.* **2011**, *23*, 1246–1251.

[10] Jiao, L. Y.; Zhang, L.; Wang, X. R.; Diankov, G.; Dai, H. J. Narrow graphene nanoribbons from carbon nanotubes. *Nature* **2009**, *458*, 877–880.

[11] Kosynkin, D. V.; Higginbotham, A. L.; Sinitskii, A.; Lomeda, J. R.; Dimiev, A.; Price, B. K.; Tour, J. M. Longitudinal unzipping of carbon nanotubes to form graphene nanoribbons. *Nature* **2009**, *458*, 872–876.

[12] Chen, C. X.; Lin, Y.; Zhou, W.; Gong, M.; He, Z. Y.; Shi, F. Y.; Li, X. Y.; Wu, J. Z.; Lam, K. T.; Wang, J. N. et al. Sub-10-nm graphene nanoribbons with atomically smooth edges from squashed carbon nanotubes. *Nat. Electron.* **2021**, *4*, 653–663.

[13] Elías, A. L.; Botello-Méndez, A. R.; Meneses-Rodríguez, D.; González, V. J.; Ramírez-González, D.; Ci, L.; Muñoz-Sandoval, E.; Ajayan, P. M.; Terrones, H.; Terrones, M. Longitudinal cutting of pure and doped carbon nanotubes to form graphitic nanoribbons using metal clusters as nanoscalpels. *Nano Lett.* **2010**, *10*, 366–372.

[14] Cai, J. M.; Ruffieux, P.; Jaafar, R.; Bieri, M.; Braun, T.; Blankenburg, S.; Muoth, M.; Seitsonen, A. P.; Saleh, M.; Feng, X. L. et al. Atomically precise bottom-up fabrication of graphene nanoribbons. *Nature* **2010**, *466*, 470–473.

[15] Liu, J. Z.; Li, B. W.; Tan, Y. Z.; Giannakopoulos, A.; Sanchez-Sanchez, C.; Beljonne, D.; Ruffieux, P.; Fasel, R.; Feng, X. L.; Müllen, K. Toward cove-edged low band gap graphene nanoribbons. *J. Am. Chem. Soc.* **2015**, *137*, 6097–6103.

[16] Ruffieux, P.; Wang, S. Y.; Yang, B.; Sánchez-Sánchez, C.; Liu, J.; Dienel, T.; Talirz, L.; Shinde, P.; Pignedoli, C. A.; Passerone, D. et al. On-surface synthesis of graphene nanoribbons with zigzag edge topology. *Nature* **2016**, *531*, 489–492.

[17] Wei, D. C.; Liu, Y. Q.; Zhang, H. L.; Huang, L. P.; Wu, B.; Chen, J. Y.; Yu, G. Scalable synthesis of few-layer graphene ribbons with controlled morphologies by a template method and their applications in nanoelectromechanical switches. *J. Am. Chem. Soc.* **2009**, *131*, 11147–11154.

[18] Jacobberger, R. M.; Kiraly, B.; Fortin-Deschenes, M.; Levesque, P. L.; McElhinny, K. M.; Brady, G. J.; Delgado, R. R.; Roy, S. S.;

Mannix, A.; Lagally, M. G. et al. Direct oriented growth of armchair graphene nanoribbons on germanium. *Nat. Commun.* **2015**, *6*, 8006.
[19] Sprinkle, M.; Ruan, M.; Hu, Y.; Hankinson, J.; Rubio-Roy, M.; Zhang, B.; Wu, X.; Berger, C.; De Heer, W. A. Scalable templated growth of graphene nanoribbons on SiC. *Nat. Nanotechnol.* **2010**, *5*, 727–731.
[20] Lu, X. B.; Yang, W.; Wang, S. P.; Wu, S.; Chen, P.; Zhang, J.; Zhao, J.; Meng, J. L.; Xie, G. B.; Wang, D. M. et al. Graphene nanoribbons epitaxy on boron nitride. *Appl. Phys. Lett.* **2016**, *108*, 113103.
[21] Xie, L. M.; Wang, H. L.; Jin, C. H.; Wang, X. R.; Jiao, L. Y.; Suenaga, K.; Dai, H. J. Graphene nanoribbons from unzipped carbon nanotubes: Atomic structures, Raman spectroscopy, and electrical properties. *J. Am. Chem. Soc.* **2011**, *133*, 10394–10397.
[22] Wang, L.; Xu, X. Z.; Zhang, L. N.; Qiao, R. X.; Wu, M. H.; Wang, Z. C.; Zhang, S.; Liang, J.; Zhang, Z. H.; Zhang, Z. B. et al. Epitaxial growth of a 100-square-centimetre single-crystal hexagonal boron nitride monolayer on copper. *Nature* **2019**, *570*, 91–95.
[23] Qin, L. C. Determination of the chiral indices (*n, m*) of carbon nanotubes by electron diffraction. *Phys. Chem. Chem. Phys.* **2007**, *9*, 31–48.
[24] Overbeck, J.; Barin, G. B.; Daniels, C.; Perrin, M. L.; Braun, O.; Sun, Q.; Darawish, R.; De Luca, M.; Wang, X. Y.; Dumslaff, T. et al. A universal length-dependent vibrational mode in graphene nanoribbons. *ACS Nano* **2019**, *13*, 13083–13091.
[25] Graf, D.; Molitor, F.; Ensslin, K.; Stampfer, C.; Jungen, A.; Hierold, C.; Wirtz, L. Spatially resolved Raman spectroscopy of single- and few-layer graphene. *Nano Lett.* **2007**, *7*, 238–242.
[26] Casiraghi, C.; Hartschuh, A.; Qian, H.; Piscanec, S.; Georgi, C.; Fasoli, A.; Novoselov, K. S.; Basko, D. M.; Ferrari, A. C. Raman spectroscopy of graphene edges. *Nano Lett.* **2009**, *9*, 1433–1441.
[27] Gupta, A. K.; Russin, T. J.; Gutiérrez, H. R.; Eklund, P. C. Probing graphene edges via Raman scattering. *ACS Nano* **2009**, *3*, 45–52.
[28] Hu, Y.; Kang, L. X.; Zhao, Q. C.; Zhong, H.; Zhang, S. C.; Yang, L. W.; Wang, Z. Q.; Lin, J. J.; Li, Q. W.; Zhang, Z. Y. et al. Growth of high-density horizontally aligned SWNT arrays using Trojan catalysts. *Nat. Commun.* **2015**, *6*, 6099.
[29] Simeonov, K.; Lederman, D. Surface structure of structure of $(11\bar{2}0)$ Al_2O_3 single crystals after high temperature annealing. *Surf. Sci.* **2009**, *603*, 232–236.
[30] Shadmi, N.; Sanders, E.; Wachtel, E.; Joselevich, E. Guided growth of horizontal single-wall carbon nanotubes on M-plane sapphire. *J. Phys. Chem. C* **2015**, *119*, 8382–8387.
[31] Li, Y. Y.; Chen, M. X.; Weinert, M.; Li, L. Direct experimental determination of onset of electron–electron interactions in gap opening of zigzag graphene nanoribbons. *Nat. Commun.* **2014**, *5*, 4311.